


Probing neutrino magnetic moments and the Xenon1T excess with coherent elastic solar neutrino scattering

Yu-Feng Li^{1,2,*} and Shuo-yu Xia^{1,2,†}

¹*Institute of High Energy Physics, Chinese Academy of Sciences, Beijing 100049, China*

²*School of Physical Sciences, University of Chinese Academy of Sciences, Beijing 100049, China*

 (Received 26 April 2022; revised 19 October 2022; accepted 24 October 2022; published 18 November 2022)

The detection potential of the active neutrino magnetic moment (ν_a MM) and the active sterile transition magnetic moment (ν_s MM) in the solar neutrino CE ν NS process from future dark matter direct detection experiments is studied and compared with the respective allowed range to explain the Xenon1T excess. We find that the sensitivity to the ν_a MM approaches to the level between $10^{-10}\mu_B$ and $10^{-11}\mu_B$, which is dominantly limited by the detection threshold. On the other hand, the future solar neutrino CE ν NS detection would be powerful in probing the ν_s MM for the sterile neutrino mass below 10 MeV, which can unambiguously test the ν_s MM explanation of the Xenon1T excess. The sensitivity in the general framework with both ν_a MM and ν_s MM contributions is also derived.

DOI: [10.1103/PhysRevD.106.095022](https://doi.org/10.1103/PhysRevD.106.095022)

I. INTRODUCTION

The observation of coherent elastic neutrino-nucleus scattering [1,2] (CE ν NS) by the COHERENT Collaboration at the spallation neutron source at Oak Ridge National Laboratory [3–5] has unlocked a new and powerful tool to explore various physics phenomena in very diverse research fields including particle physics [6–10], nuclear physics [11,12], astrophysics [13–15], and cosmology [16]. The CE ν NS process provides an innovative access to investigate the nuclear neutron density distributions [11,12,17–20] as well as the weak mixing angle [8,21] and the neutrino electromagnetic properties [22–24]. Besides, CE ν NS can be a new play ground for the new physics beyond the Standard Model (SM) [6–10,13,14,16,22–27].

CE ν NS experiments based on the neutrino fluxes from artificial sources including the spallation neutron source [28,29] and nuclear reactors [30–35] are promising on providing competitive constraints on a series of the new physics theories. On the other hand, there have been intensive interests in the observation of astrophysical neutrino fluxes through the CE ν NS process, which could be a new probe to the supernovae [36–41], the collapsing supermassive stars [42] and the primordial black holes [43].

Solar neutrinos, which have already been observed with the charged-current (CC) [44–49], neutral current (NC) [50–52] and elastic scattering (ES) [53–59] channels, and provide a stable flux for CE ν NS experiments as one of the most intensive natural neutrino sources at the Earth. Meanwhile, the recoil energy region of the solar neutrino CE ν NS process is located at the same target range of direct detection (DD) experiments with weakly interacting massive particles (WIMPs) as the promising dark matter candidate, making it an important component of the neutrino floor [60–65], as well as a suitable target signal for detection.

Recently, the Xenon1T Collaboration released the recoiled electron spectrum in the dark matter searches and observed an unexplained excess of 53 ± 15 events above the expected background at a statistical significance of around 3σ [66].¹ This excess is reported to be consistent with the solar neutrino ES process due to the active neutrino magnetic moment (ν_a MM) in the region of $(1.4, 2.9) \times 10^{-11}\mu_B$ [66,68,69], which is close to the current best limit reported by the Borexino Collaboration [70]. However it is stringently limited by indirect constraints from analyses of white dwarfs [71], red-giants [72] and globular clusters [73], which have constrained the ν_a MM at the level of $10^{-12}\mu_B$. Another appealing solution is the active-sterile transition magnetic moments (ν_s MM), also known as neutrino dipole portal [74–78], which is capable to explain

*liyufeng@ihep.ac.cn

†Corresponding author.
xiashuoyu@ihep.ac.cn

Published by the American Physical Society under the terms of the [Creative Commons Attribution 4.0 International license](https://creativecommons.org/licenses/by/4.0/). Further distribution of this work must maintain attribution to the author(s) and the published article's title, journal citation, and DOI. Funded by SCOAP³.

¹The new publication [67] of the Xenon-nT experiment does not confirmed Xenon-1T excess but attributes the excess to the possible background from Tritium decays. This new result has in turn placed stringent constraints on the neutrino magnetic moments, and indeed demonstrated the excellent prospects of neutrino property studies in future DD experiments.

the Xenon1T excess [79–83], and still compatible with the laboratory and astrophysical bounds [16]. At present, dark matter DD experiments are entering the phase of the multiton scale and experiments like PandaX-4T [84], DARWIN [85] and DarkSide-20k [86] can be an effective platform to detect CE ν NS process due to lower energy threshold and higher target material mass. In addition, experiments employing germanium or silicon as the target material like SuperCDMS [87] and EDELWEISS [88] have achieved an extremely low threshold, which will significantly improve the efficiency to probe possible new physics beyond the SM. Therefore, CE ν NS process in DD experiments can be another access to explore the explanations for the Xenon1T excess.

In this work, we are going to study the detection potential of the ν_a MM and ν_s MM with the solar neutrino CE ν NS detection in the next generation and future DD experiments. We present the sensitivity of the ν_a MM and ν_s MM, and compare with the allowed range to explain the Xenon1T excess and other experimental constraints. We find that the sensitivity to the ν_a MM lies in the level of $[10^{-10}, 10^{-11}]\mu_B$, which is dominantly limited by the detection threshold. Only the future silicon detector could match the allowed region to explain the Xenon1T excess. On the other hand, the solar neutrino CE ν NS would be powerful in probing the ν_s MM for the sterile neutrino mass below 10 MeV. All the considered scenarios can unambiguously test the ν_s MM explanation of the Xenon1T excess with at least one order of magnitude better detection sensitivities. We also derive the detection potential in the general framework with both ν_a MM and ν_s MM contributions in the CE ν NS process.

The plan of this work is as follows. In Sec. II, we briefly describe the theoretical calculation of the CE ν NS cross section in the presence of the ν_a MM and ν_s MM. In Sec. III, we illustrate the setup of the experimental scenarios and statistical analysis method. In Sec. IV, we present the numerical constraints. Finally we give the concluding remarks in Sec. V.

II. THEORETICAL FRAMEWORK

To begin with, we illustrate the theoretical calculation of the CE ν NS cross section under the SM and in the presence of the neutrino magnetic moment (ν MM). The cross section in this case can be written as [89,90]

$$\frac{d\sigma}{dT}(E_\nu, T) = \frac{d\sigma_{\text{SM}}}{dT}(E_\nu, T) + \frac{d\sigma_{\nu\text{MM}}}{dT}(E_\nu, T), \quad (2.1)$$

where $d\sigma_{\text{SM}}/dT$ is the differential cross section of the CE ν NS process between a neutrino with the energy E_ν and a nucleus with Z protons and N neutrons in the SM and can be written as

$$\frac{d\sigma_{\text{SM}}}{dT}(E_\nu, T) = \frac{G_F^2 M}{\pi} \left(1 - \frac{MT}{2E_\nu^2}\right) \times [g_V^p Z F_Z(q^2) + g_V^n N F_N(q^2)]^2, \quad (2.2)$$

where T is the kinetic energy of nuclear recoil, M is the nucleus mass and G_F is the Fermi constant. g_V^p and g_V^n are the vector neutrino-proton and neutrino-neutron couplings respectively, which can be written as

$$g_V^p = -2 \sin^2 \theta_W + \frac{1}{2} \simeq 0.0229, \quad g_V^n = -\frac{1}{2}, \quad (2.3)$$

where θ_W is the weak mixing angle at low momentum transfer with $\sin^2 \theta_W = 0.23857$ [91] and the radiative corrections have been neglected [17]. Meanwhile, $F_Z(q^2)$ and $F_N(q^2)$ are the form factors of nucleon distributions in the nucleus for proton and neutron respectively and $q^2 = |\vec{q}|^2 = 2MT$ is the square of momentum transfer. In this work, we use the Helm parametrization [92] for the form factors of all considered nuclei and neglect the difference between proton and neutron form factors. The Helm proton form factor can be written as

$$F_Z(q^2) = 3 \frac{j_1(qR_Z)}{qR_Z} e^{-q^2 s^2/2}, \quad (2.4)$$

where the surface thickness $s = 0.9$ fm and the proton radii R_Z from Ref. [93] have been employed for the target nuclei in the following calculation. Note that the cross section will be weighted averaged according to the natural abundance if there are several stable isotopes for the target material.

The general form of the CE ν NS cross section induced by the ν MM for a neutrino mass eigenstate with the mass m_i scattered to the mass eigenstate with mass m_j can be written in a similar form as that of the electron scattering process [83]:

$$\frac{d\sigma_{\nu\text{MM}}^{ij}}{dt} = \frac{e^2}{8\pi\lambda} \left| \frac{\mu_{ij}}{\mu_B} \right|^2 Z^2 F_Z^2(q^2) \left[\frac{1}{t} (2\lambda + 4M^2 m_i^2 + 2A\Delta + 2M^2\Delta + \Delta^2) + (2A + \Delta) + \frac{2M^2\Delta^2}{t^2} \right] \quad (2.5)$$

where μ_{ij} is the neutrino magnetic moment connecting the mass eigenstates of ν_i and ν_j , μ_B is the Bohr Magnetron, and

$$A = s - M^2 - m_i^2, \quad \Delta = m_i^2 - m_j^2, \quad \lambda = A^2 - 4M^2 m_i^2, \quad (2.6)$$

with s and t being the Mandelstam variables, and in the laboratory frame are given by

$$s = M^2 + m_i^2 + 2ME_\nu \quad \text{and} \quad t = -2MT. \quad (2.7)$$

Note that the neutrino mass eigenstates with $(i, j = 1, 2, 3, 4)$ include three kinds of active neutrinos and one sterile neutrino ν_4 .

In this work, we consider the CE ν NS process with solar neutrinos scattered to either the active or heavy sterile neutrino eigenstates. Therefore, the matrix of neutrino magnetic moments μ_{ij} can be written as

$$(\mu_{ij}) = \left(\begin{array}{ccc|c} \mu_{11} & \mu_{12} & \mu_{13} & \mu_{14} \\ \mu_{21} & \mu_{22} & \mu_{23} & \mu_{24} \\ \mu_{31} & \mu_{32} & \mu_{33} & \mu_{34} \\ \hline \mu_{41} & \mu_{42} & \mu_{43} & \mu_{44} \end{array} \right), \quad (2.8)$$

where the top-left part is the matrix of the active neutrino magnetic moment (ν_a MM) and the left-bottom and right top parts are the active-sterile transition magnetic moment (ν_s MM). The right bottom part μ_{44} is the diagonal magnetic moment in the elastic scattering of the sterile neutrino ν_4 . Note that we have neglected the flavor mixing between active and sterile neutrinos, thus there is no sterile neutrino component in the solar neutrino flux, and ν_4 can only be generated by neutrino upscattering via the ν_s MM. Note that although the elements of the magnetic moment matrix are complex, the effective magnetic moment relevant for the solar neutrino observation in DD experiments is independent of possible CP effects.

In the CE ν NS process considered in this work, the electron neutrino produced near the solar core is a superposition of three active neutrino mass states and the magnetic moment at the detection is an effective magnetic moment with the neutrino mixing and flavor oscillation considered, which is given by [13,83]

$$\mu_{\text{Solar}}^2(L, E_\nu) = \sum_l \left| \sum_{k=1}^3 (U_{ek}^M)^* e^{-i\Delta m_{kl}^2 L/2E_\nu} \mu_{lk} \right|^2, \quad (2.9)$$

where U_{ek}^M is the mixing matrix element at the neutrino production in the solar core, and $\Delta m_{kl}^2 \equiv m_k^2 - m_l^2$ is the mass squared difference of neutrino mass eigenstates. Since the distance L between the Sun and the Earth is much larger than the oscillation lengths, the interference terms $e^{-i\Delta m_{kl}^2 L/2E_\nu}$ are washed out during the measurement. Then the effective magnetic moment at the detection can be written as

$$\begin{aligned} \mu_{\text{Solar}}^2(E_\nu) &= \sum_{k=1}^3 |U_{ek}^M|^2 \sum_l |\mu_{lk}|^2 \\ &\equiv \sum_\alpha |\mu_{\nu_\alpha}|^2 \left[\sum_{k=1}^3 |U_{ek}^M|^2 |U_{\alpha k}|^2 \right] \\ &\equiv |\mu_{\nu_e}|^2 \left[\sum_{k=1}^3 |U_{ek}^M|^2 |U_{ek}|^2 \right] \\ &\quad + |\mu_{\nu_{\mu\tau}}^{\text{eff}}|^2 \sum_{\alpha=\mu,\tau} \left[\sum_{k=1}^3 |U_{ek}^M|^2 |U_{\alpha k}|^2 \right], \quad (2.10) \end{aligned}$$

where μ_{ν_α} is the effective magnetic moment of the flavor neutrino ν_α . Since the electron neutrinos produced in the solar core turn into the fluxes with ν_e , ν_μ , and ν_τ through neutrino oscillations when arrive at the Earth, in this work we consider the electron neutrino magnetic moment μ_{ν_e} and an effective magnetic moment $\mu_{\mu\tau}^{\text{eff}}$ for ν_μ and ν_τ , which can be expressed as [69]

$$\begin{aligned} (\mu_{\nu_{\mu\tau}}^{\text{eff}})^2 &= \frac{|\mu_{\nu_\mu}|^2 [\sum_{k=1}^3 |U_{ek}^M|^2 |U_{\mu k}|^2] + |\mu_{\nu_\tau}|^2 [\sum_{k=1}^3 |U_{ek}^M|^2 |U_{\tau k}|^2]}{\sum_{\alpha=\mu,\tau} [\sum_{k=1}^3 |U_{ek}^M|^2 |U_{\alpha k}|^2]}. \quad (2.11) \end{aligned}$$

In the solar neutrino CE ν NS detection, the neutrino energy E_ν and the nuclear recoil energy T are much larger than the present upper limit of the active neutrino masses and the relevant variable Δ can be neglected. Therefore, considered the effective magnetic moment μ_{ν_α} with flavor $\alpha = e, \mu, \tau$ described above and Eq. (2.5), the popular cross section with the active ν_α magnetic moment at low energies can be written as [13,17,69,94]

$$\frac{d\sigma_{\nu_\alpha\text{MM}}}{dT} = \frac{\pi\alpha_{\text{EM}}^2}{m_e^2} Z^2 F_Z^2(q^2) \left| \frac{\mu_{\nu_\alpha}}{\mu_B} \right|^2 \left(\frac{1}{T} - \frac{1}{E_\nu} \right), \quad (2.12)$$

where m_e is the electron mass and α_{EM} is fine structure constant. $F_Z(q^2)$ is the Helm form factor and only the protons contribute to this scattering process. In this work, since there is no mixing between the active and sterile neutrinos in this model, the effective magnetic moment of neutrinos arriving at the detector only contains the active neutrino contributions [95] as shown in Eq. (2.9). This component will contribute to the scattering off the active neutrinos. On the other hand, the active-sterile magnetic moments will contribute to the upscattering off the sterile neutrinos.

Next for the ν_s MM scenario, an active neutrino ν_l upscattering to a heavy sterile neutrino ν_4 can be described with the μ_{l4} part in the Eq. (2.8). In this work, we assume that all active neutrinos universally couple to ν_4 through the dipole process and we define a universal magnetic moment in this process with the variable d given by

$$d^2 = \frac{\pi\alpha_{\text{EM}}}{m_e^2} \left| \frac{\mu_{\nu_{l4}}}{\mu_B} \right|^2, \quad (2.13)$$

where $\mu_{\nu_{l4}}$ is the active sterile transition magnetic moment in Eq. (2.8), and the parameter d is usually used in literatures as the coefficient of the effective Lagrangian [74,76]

$$\mathcal{L} = d\bar{\nu}_l \sigma^{\mu\nu} \nu_4 F_{\mu\nu} + \text{H.c.}, \quad (2.14)$$

where ν_4 is the sterile neutrino field and $F_{\mu\nu}$ is the electromagnetic field strength tensor. Note that both $\mu_{\nu_{l4}}$

and d describe the strength of the ν_s MM and they are connected through Eq. (2.13). Taking Eq. (2.5) and neglecting the active neutrino masses the cross section induced by the ν_s MM at low energies can be written as [16,79]

$$\begin{aligned} \frac{d\sigma_{\nu_s\text{MM}}}{dT} &= d^2 \alpha_{\text{EM}} Z^2 F_Z^2(q^2) \left(\frac{1}{T} - \frac{1}{E_\nu} \right. \\ &\quad \left. - \frac{m_4^2}{2E_\nu MT} \left(1 - \frac{M-T}{2E_\nu} \right) - \frac{m_4^4(M-T)}{8E_\nu^2 M^2 T^2} \right). \end{aligned} \quad (2.15)$$

Note that this cross section can return to the popular form of Eq. (2.12) when $m_4 = 0$ is taken.

III. NUMERICAL FRAMEWORK

In this section, we are going to present the statistical method and setup of the simplified experimental scenarios [27] we have employed to analyze the sensitivity of next generation and future dark matter DD experiments to the ν_a MM and ν_s MM.

A. Statistical method

In this work we discuss the solar neutrino CE ν NS process in the presence of the ν_a MM and ν_s MM. The predicted CE ν NS event rate N_i in each nuclear-recoil energy-bin is given by

$$N_i = \frac{\epsilon}{M} \int_{T_{i,\min}}^{T_{i,\max}} dT \int_{E_{\min}}^{E_{\max}} dE_\nu \cdot \Phi(E_\nu) \frac{d\sigma}{dT}, \quad (3.1)$$

where ϵ is the exposure of the considered experiment and M is the mass of the target nucleus, $\Phi(E_\nu)$ is the solar neutrino fluxes from the standard solar model BS05(OP) (SSM) [96–98]. E_{\max} is the maximal neutrino energy from the solar neutrino spectrum. E_{\min} the minimal neutrino energy for a certain recoil energy T . For the CE ν NS process with the ν_a MM, it is given by

$$E_{\min} = \frac{T}{2} \left(1 + \sqrt{1 + 2\frac{M}{T}} \right). \quad (3.2)$$

For the ν_s MM case, E_{\min} is higher due to the final heavy neutrino state ν_4 with a mass m_4 and can be written as

$$E_{\min} = \frac{m_4^2 + 2MT}{2[\sqrt{T(T+2M)} - T]}. \quad (3.3)$$

To explore the constraints on the ν_a MM and ν_s MM from the solar neutrino CE ν NS process with certain DD experiments, we employ the standard least squares method with the Asimov datasets [99]

$$\begin{aligned} \chi^2 &= \sum_{i=1}^n \left(\frac{N_i^{\text{exp}} - (1 + \epsilon_{\text{exp}}) N_i^{\text{pred}} [(1 + \epsilon_j) \Phi_{\text{SSM}}^j]}{\sigma_i} \right)^2 \\ &\quad + \left(\frac{\epsilon_{\text{exp}}}{\sigma_{\text{exp}}} \right)^2 + \sum_j \left(\frac{\epsilon_j}{\sigma_{\Phi_{\text{SSM}}^j}} \right)^2, \end{aligned} \quad (3.4)$$

where $\sigma_i^2 = N_i^{\text{exp}} + N_i^{\text{bg}}$, N_i^{exp} is the pseudo event number of the signal of the considered experiment in the i th energy bin, N_i^{pred} is the predicted event number, and N_i^{bg} is the number of background events. ϵ_{exp} is the simplified nuisance parameter which quantifies the total detection uncertainty of the experiment and σ_{exp} is the corresponding standard deviation. ϵ_j and $\sigma_{\Phi_{\text{SSM}}^j}$ are the nuisance parameter and uncertainty of the j th solar neutrino flux from the SSM, in which the largest one is 11.6% for the ^8B neutrino flux. All the nuisance parameters will be varied to minimize the χ^2 function. It is noteworthy that the quenching effect connecting the nuclear recoil to electron recoil response will be employed as described in the following subsection.

B. Experimental scenarios

Today the DD experiments are entering the phase of the multiton scale and there are considerable experiments that have the potential for the neutrino CE ν NS detection and to explore the neutrino nonstandard interactions. In the following, we summarize experimental scenarios with various target materials and detection technologies based on next generation and future DD experiments:

- (i) First, DD experiments with the liquid noble gas as the target have already achieved considerable results of the dark matter searches [100–104]. Xenon-based experiments including PandaX-4T [84], XENON-nT [105], and LZ [106] have already deployed targets of the multiple ton scale and been able to observe the CE ν NS process with solar neutrinos. In the future, DARWIN [85] will be able to deploy an unprecedented scale of target with 50 tons of liquid xenon and is promising to provide improved potential on WIMPs as well as the neutrino CE ν NS process. Argon-based experiments are capable of detecting neutrinos with relatively lower energies due to the lighter mass of the argon nucleus and a higher production of liquid argon makes a larger scale of the detection target possible. Darkside-20k [86] is planned to deploy 40 ton liquid argon for the dark matter and solar neutrino detection and ARGO [107] will increase the mass of liquid argon target to 400 tons in the future.
- (ii) Second, low threshold dark matter detectors [108–113] with the low scale solid material target can give constraints on low mass WIMPs. Next generations of this kind experiments, including Super CDMS [87], EDELWEISS-III [88], and SENSEI [114], have the potential of detecting solar neutrino CE ν NS events with extremely low recoil

TABLE I. Experimental scenarios and their typical parameters employed in this work.

Type	Target	Exposure (t × year)	Threshold (keV _{NR})	Background (t ⁻¹ year ⁻¹ keV ⁻¹)
Ge-Next generation	Germanium	0.2	0.1	1
Si-Next generation	Silicon	0.2	0.1	1
Xe-Next generation	Xenon	20	3.5	2
Ar-Next generation	Argon	200	3.5	2
Ge-future	Germanium	2	0.04	1
Si-future	Silicon	2	0.04	1
Xe-future	Xenon	200	1	2
Ar-future	Argon	3000	1	2

energies and may provide more severe tests for new physics beyond the SM.

Based on the above investigation, we have designed the experimental scenarios listed in Table I with four target materials, where next generation indicates the experiments in the coming years and Future represents those in the far future with the comprehensively improved detection technologies. In the table, the detection exposure, the energy threshold, and the background level are provided for each experimental scenario. For each scenario, we consider a nominal systematic uncertainty of $\sigma_{\text{exp}} = 10\%$ and an optimistic systematic uncertainty of $\sigma_{\text{exp}} = 5\%$ to show the effects of different systematic uncertainties on the sensitivity results. We use a simplified flat background level for an economic computing resource budget based on the consideration in Refs. [87,103,115], which are also listed in Table I. The upper bound for our analysis is 10 keV_{NR} and signals submerge in background above this bound.

In the CE ν NS process, the recoil energy of a nucleus will only be partly converted into the ionization energy E_{ion} [98], which can be directly detected in DD experiments and this quenching effect can be illustrated as $E_{\text{ion}} = YT$, where T is the nuclear recoil energy and Y is the quenching factor. At high energies, the quenching factor can be theoretically estimated by the Lindhard model [116] as

$$Y_L(T) = \frac{kg(\epsilon)}{1 + kg(\epsilon)}, \quad (3.5)$$

where $g(\epsilon) = 3\epsilon^{0.15} + 0.7\epsilon^{0.6} + \epsilon$ and $\epsilon = 11.5Z^{-7/3}T$, Z is the proton number and the nuclear recoil energy T is

given in keV. The original theory by Lindhard sets $k = 0.133Z^{2/3}A^{-1/2}$, where A is the mass number of the nucleus, but experimental data indicate a range of values under different recoil energies. For silicon and germanium targets, fitting results for the quenching factor from Ref. [98] with high ionization efficiency are employed and k is set to 0.15 and 0.2 respectively for high recoil energies. In contrast, the linear quenching factors are used for smaller recoil energy regions. For the liquid argon target, we have adopted the linear quenching factor from simultaneous fits based on CENNS-10 from Ref. [4], and for the liquid xenon target we use the original Lindhard model [117]. The expressions for quenching factors employed in this work are listed in Table II.

IV. NUMERICAL RESULTS

In this section we present numerical analysis results. First, we show the predicted event spectra for each experimental scenario as a function of the equivalent electron recoil energy. Then we illustrate the sensitivity of the solar neutrino CE ν NS detection on the ν_a MM and ν_s MM in different experimental scenarios. We have also considered the general case with both the ν_a MM and ν_s MM to show what are the remaining parameter space with the solar neutrino CE ν NS detection.

A. Predicted event spectra

In Fig. 1 we show the predicted event energy spectra as a function of the nuclear recoil ionization energy for different detector materials in the presence of ν_a MM (left panel) and

TABLE II. Quenching factors employed in this work.

Target	Recoil energy T (eV _{NR})	Quenching factor Y
Liquid argon [4]	1000–10000	$0.246 + (7.8 \times 10^{-4} \text{ keV}_{\text{NR}}^{-1})T$
Liquid xenon [117]	1000–10000	$Y_L(T), k = 0.133Z^{2/3}A^{-1/2}$
Germanium [98]	40–250	$0.18[1 - e^{-(T[\text{eV}_{\text{NR}}^{-1}] - 15)/71.3}]$
	250–10000	$Y_L(T), k = 0.2$
Silicon [98]	40–254	$0.18[1 - e^{-(T[\text{eV}_{\text{NR}}^{-1}] - 15)/71.03}]$
	254–10000	$Y_L(T), k = 0.15$

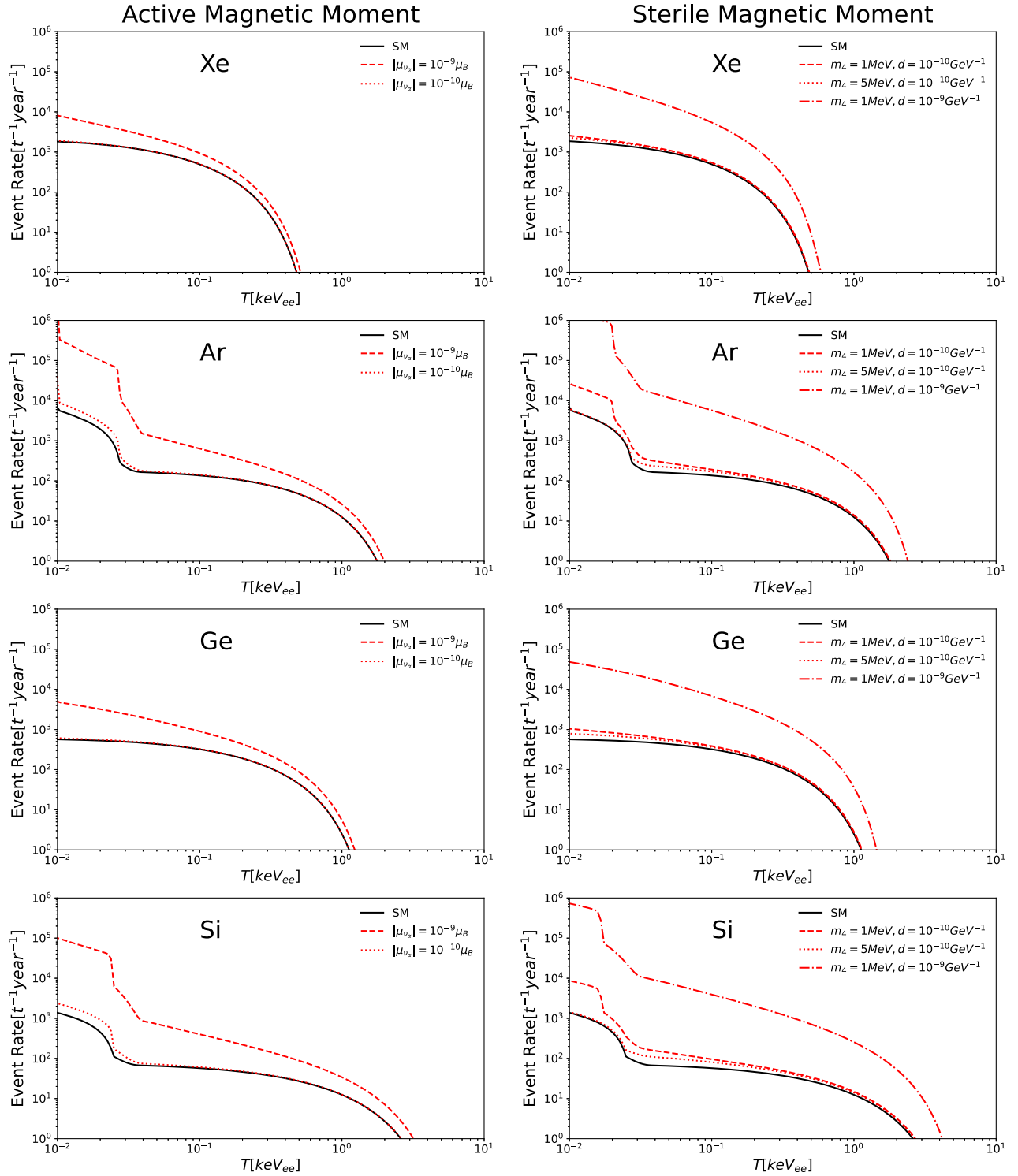


FIG. 1. Predicted event energy spectra as a function of the nuclear recoil ionization energy for different detector materials in the presence of the ν_a MM (left panel) and ν_s MM (right panel) and with the quenching effect. A weighted average have been performed according to the natural abundance of isotopes in the detector material. From top to bottom rows results are shown for xenon, argon, germanium, and silicon detectors respectively.

ν_s MM (right panel) and with the quenching effect. A weighted average have been performed according to the natural abundance of isotopes in the detector material. From top to bottom rows results are shown for xenon,

argon, germanium, and silicon detectors, respectively. Since both contributions of the ν_a MM and ν_s MM are suppressed by the recoil energy T as shown in Eqs. (2.12) and (2.15), these effects would become significant when

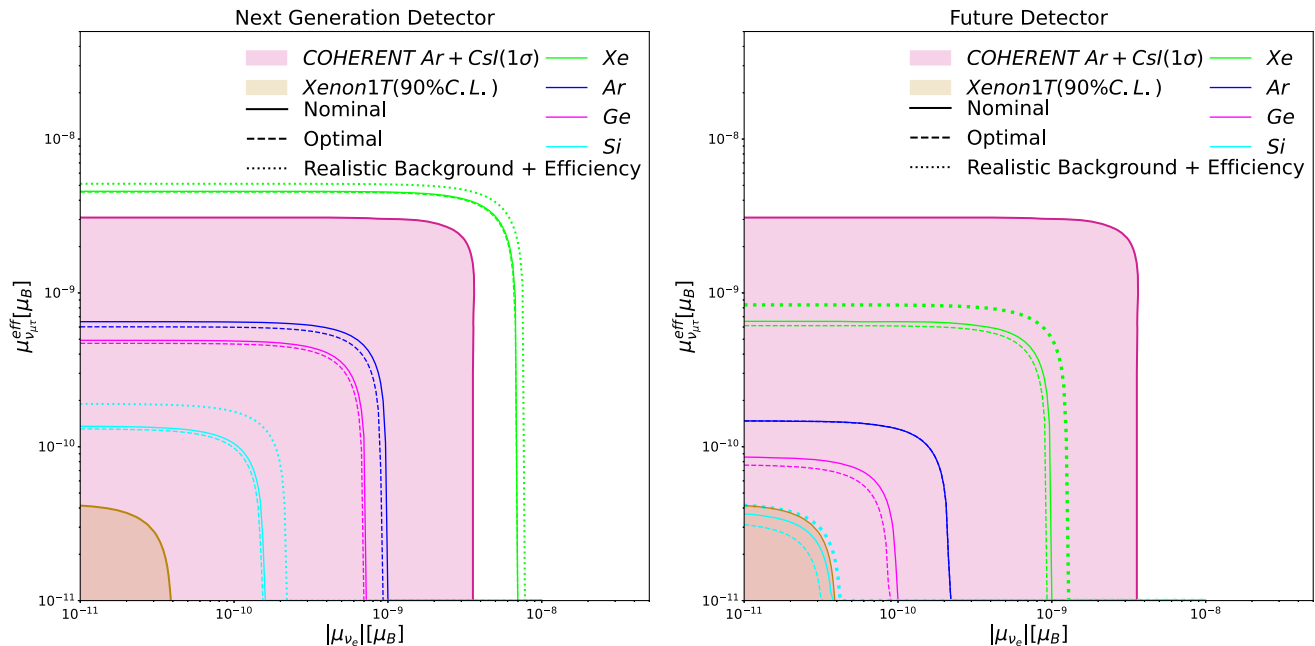


FIG. 2. 90% confidence level (CL) upper limits on the parameter space of ν_a MM from the experimental scenarios listed in Table I, where the solid lines are for the nominal systematic uncertainty and dashed lines for the optimal systematic uncertainty. We have also shown with dotted lines the results with realistic backgrounds from Xenon1T [105] and SuperCDMS [87] for xenon and silicon detectors respectively, and with realistic efficiencies [120,121] under a nominal uncertainty of 10%. The left and right panels are shown for the next generation and future experimental scenarios, respectively. A weighted average have been performed according to the natural abundance of isotopes in detector material. The allowed region from the Xenon1T excess [66,69] and constraint from the combined analysis of COHERENT Ar and CsI data [17] are also shown for comparison.

the recoil energy decreases and low threshold experiments are needed for improved exploration. The discontinuities on the spectra of argon and silicon detectors below 0.1 keV_{ee} are from the appearance of the CNO neutrino flux, which can be explained by using Eq. (3.2). There is no such discontinuity on the spectra of xenon and germanium detectors because of heavier nucleus masses. Several comments on the spectra are provided as follows.

- (i) For the ν_a MM case, we have shown the relevant contribution with the neutrino magnetic moment μ_{ν_l} of all flavors set to $10^{-9}\mu_B$ and $10^{-10}\mu_B$, respectively. The contribution of the ν_a MM is proportional to the square of μ_{ν_l} and the magnetic moment of $10^{-10}\mu_B$ or smaller is extremely hard to probe even with the 10 eV threshold for xenon and germanium targets. Lighter nuclei like argon and silicon have visible sensitivity for the 10 eV_{ee} threshold due to relatively high recoil energies.
- (ii) The contribution of the ν_s MM is similar to that of the ν_a MM case while the mass of the sterile neutrino significantly suppresses the event rates due to the minimal energy required for solar neutrinos to up-scatter a heavy sterile one as shown in Eq. (3.3). Therefore, effects of the ν_s MM are completely suppressed at low recoil energies as shown in several tens of eV in the energy spectra with argon and

silicon as targets. For liquid xenon and germanium targets this phenomenon will happen at the lower recoil energies because of heavier nuclear masses.

B. Constraints on the ν_a MM and ν_s MM

In Figs. 2 and 3 we have illustrated the 90% confidence level (CL) upper limits on the parameter space of the ν_a MM and ν_s MM with the experimental scenarios listed in Table I respectively. The solid lines are for the nominal systematic uncertainty and dashed lines for the optimal systematic uncertainty. The left and right panels are shown for next generation and future experimental scenarios respectively and the natural abundance of isotopes has been taken into consideration with corresponding weighted average. The allowed regions of the Xenon1T excess at 90% CL in Ref. [69,118] are illustrated as colored bands. Meanwhile the constraints from the combined analysis of COHERENT Ar and CsI data [17], from Borexino [16], $\nu_s \rightarrow \nu\gamma$ [81], TEXONO [118,119] are also shown for comparison. Apart from the simplified flat background, we have also employed realistic backgrounds for xenon and silicon detectors from Xenon1T [105] and SuperCDMS [87] respectively, and with realistic efficiencies [120,121] under a nominal uncertainty of 10%, which are shown in dotted lines.

It is shown in Figs. 2 and 3 that the silicon target provides significantly more stringent constraints than others for the

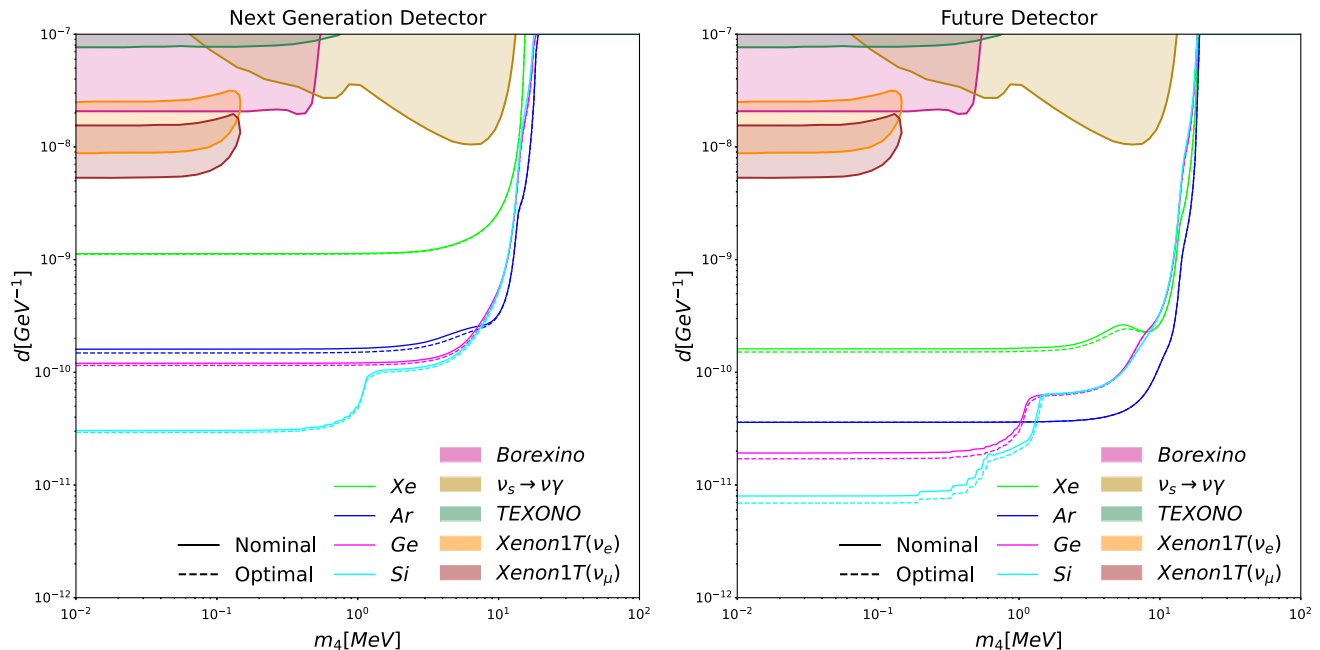


FIG. 3. 90% confidence level (CL) upper limits on the ν_s MM parameter space from the experimental scenarios listed in Table. I, where the solid lines are for the nominal systematic uncertainty and dashed lines for the optimal systematic uncertainty. The left and right panels are shown for the next generation and future experimental scenarios, respectively. A weighted average have been performed according to the natural abundance of isotopes in detector material. The allowed region from the Xenon1T excess [66,118], and the present experimental constraints from Borexino [16], TEXONO [118,119] and the $\nu_s \rightarrow \nu\gamma$ decay sensitivity from Borexino and Super Kamiokande [81] are shown for comparison.

lightest nuclear mass and lowest detection threshold. Constraints from experiments with liquid argon and germanium as targets are more stringent than that of xenon-based experiments for higher exposure and better threshold respectively. It can be revealed that the contribution of better systematic uncertainty only take effects with enough exposure and threshold, which is the case of argon-based next generation experiments and future experiments with xenon, germanium and silicon as targets. However, improving systematic uncertainty may suffer from marginal effects when the threshold and statistics are below a certain level as shown in xenon-based next generation experiments, where the improvement of the systematic uncertainty shows little effect and the upper limits with different systematic uncertainties coincide with each other. For the results of next generation setups with realistic backgrounds, a much lower background of xenon experiments produces better results while higher backgrounds leads to worse constraints for solid detectors. For the results of future setups, the extremely large exposure will minimize the effects of backgrounds and the realistic backgrounds produce similar results with that by flat backgrounds. For the results with realistic backgrounds and efficiencies, the capabilities to constrain the neutrino magnetic moment under different setups are all weakened. Some relevant comments are summarized as follows:

- (i) For the ν_a MM, the next generation experiments give constraints at the level of $\mathcal{O}(10^{-10})\mu_B$ except for

xenon-based experiments, which are better than the limit from the combined analysis of COHERENT Ar and CsI data [17]. Future experimental scenarios provide significantly more stringent constraints and liquid noble gas based and low threshold solid based experiments are capable of the μ_{ν_l} limit to the $\mathcal{O}(10^{-10})\mu_B$ and $\mathcal{O}(10^{-11})\mu_B$ levels respectively. It should be noticed that only future experiments with silicon as the target have the potential to exclude the parameter space to explain the excess from electron recoil results of Xenon1T [66].

- (ii) It is shown in Fig. 3 that the CE ν NS detection in DD experiments provides excellent constraints on the ν_s MM model, and both next generation and future experimental scenarios can unambiguously test the parameter space from the Xenon1T excess [66]. Meanwhile, constraints from these experiments are significantly better than present experimental constraints from Borexino [16], TEXONO [118,119] and the $\nu_s \rightarrow \nu\gamma$ decay sensitivity from Borexino and Super Kamiokande [81]. Note that there are several sudden changes in the sensitivity curves of silicon-based experiments and future germanium-based experiments, which are resulted from the appearance of different low-energy solar neutrino fluxes. With the recoil energy threshold, the target nuclear mass and sterile neutrino mass considered, it can be easily concluded from the minimal neutrino energy to

trigger the ν_s MM process in Eq. (3.3) that the lower sudden changes of future silicon-based curves are from the appearance of the ${}^7\text{Be}$ neutrino flux and the presence of CNO neutrino fluxes leads to the other sudden changes. Meanwhile, the ${}^8\text{B}$ neutrino flux contributes to the constraints with higher sterile neutrino masses, but the pp and $0.384\text{ MeV } {}^7\text{Be}$ neutrino fluxes are not able to provide the constraints beyond 10 eV due to lower recoil energies.

- (iii) Comparing between Figs. 2 and 3, one can conclude that the $\text{CE}\nu\text{NS}$ process in DD experiments provides far more stringent constraints on the ν_s MM than the electron neutrino elastic scattering ($\text{E}\nu\text{ES}$) while weaker for the case of the ν_a MM. In the presence of the ν_a MM, $\text{E}\nu\text{ES}$ induces significantly more events than $\text{CE}\nu\text{NS}$ with advantages of both higher event rate at most recoil energies and a much larger allowed recoil energy range. In the presence of the ν_s MM, the situation becomes more complicated since the minimal neutrino energies to trigger the up-scattering are not monotone increasing. It can be easily observed from Eq. (3.3) and Fig. 5 that the minimal neutrino energy E_{\min} continuously decreases as the increase of the recoil energy T , until E_{\min} reaches the extreme value $E_{\min} = m_4 + m_4^2/2M$ at $T = m_4^2/2(m_4 + M)$, where M is the mass for the target electrons or nuclei and m_4 is the sterile neutrino mass. After the minimal neutrino energy reaches the extreme value, it will start to increase as the recoil energy. As shown in Fig. 5, with a higher sterile neutrino mass, $\text{CE}\nu\text{NS}$ provides

a significantly lower energy threshold for the initial neutrino than $\text{E}\nu\text{ES}$ at nearly all recoil energies in the energy range of the practical analysis. However, as the sterile neutrino mass is decreasing, the initial neutrino energy threshold in $\text{E}\nu\text{ES}$ will decrease faster. With a sterile neutrino of 0.1 MeV , $\text{E}\nu\text{ES}$ provides a lower energy threshold of the initial neutrino for most of the recoil energy. When the mass of the sterile neutrino reaches zero, the case will be degenerate to that of the ν_a MM, where $\text{E}\nu\text{ES}$ provides better constraints on the magnetic moment. Such phenomenon also appeared in earlier studies in the case of ${}^{51}\text{Cr}$ in Ref. [118].

- (iv) It has been shown in Fig. 2 that the constraints of the ν_a MM can hardly reach the parameter space of the Xenon1T excess using the considered experimental scenarios. Therefore in Fig. 4 we further illustrate the requirements of different target materials to reach the ν_a MM sensitivity with $\mu_{\nu_l} = 10^{-11}\mu_B$ (90% CL) as functions of the exposure and detection threshold. In the left panel, the jump of the xenon detector and the left jump of the argon detector result from the maximum threshold to detect the peak of the ${}^7\text{Be}$ flux at 0.384 MeV , while the right jump of the argon detector is from the maximum threshold to detect the pp flux. It is clearly that within the feasible exposure range at present or in the near future, extremely low threshold is needed to efficiently constrain the ν_a MM compared to the $\text{E}\nu\text{ES}$ experiments. However, the atomic effects studied in Refs. [122–125] may significantly affect the results, which need

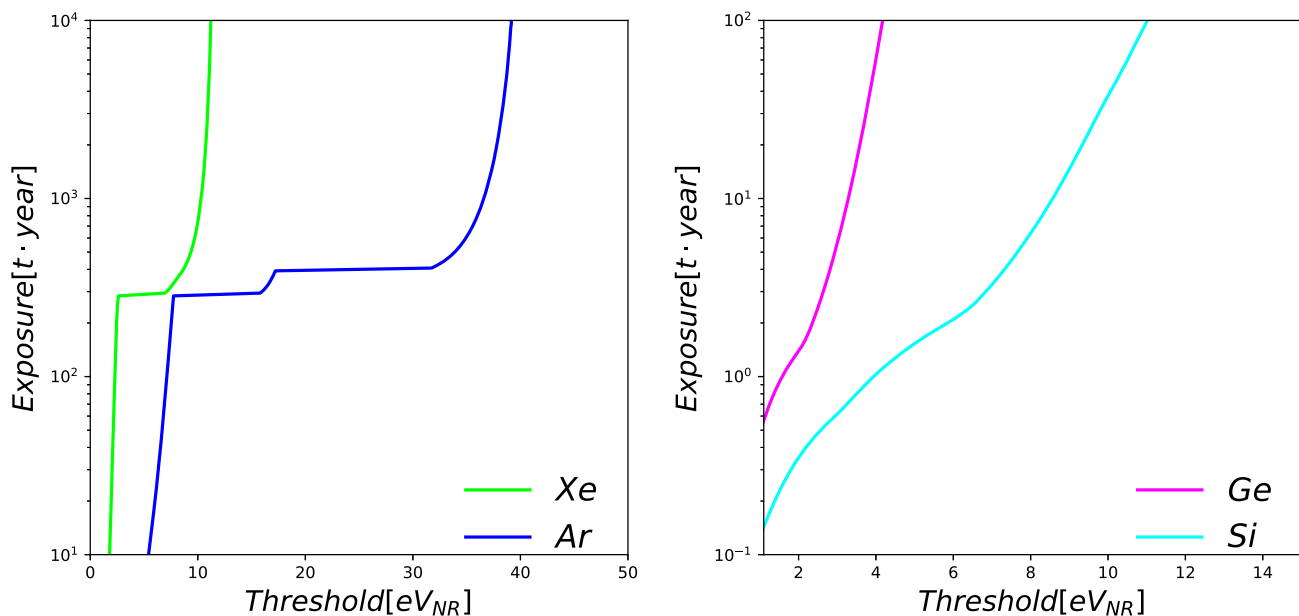


FIG. 4. Requirements to reach the ν_a MM sensitivity of $\mu_{\nu_l} = 10^{-11}\mu_B$ (90% CL) as the function of the exposure and detection threshold for different target materials.

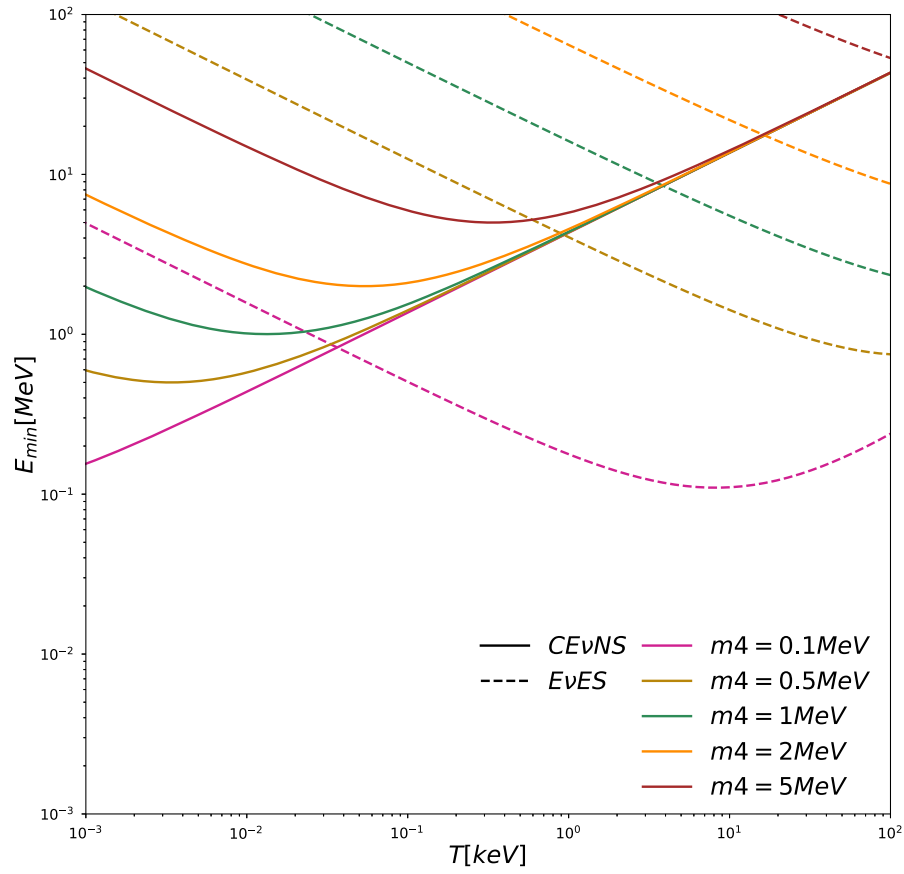


FIG. 5. Minimal neutrino energy in the presence of the ν_s MM according to Eq. (3.3) for different sterile neutrino masses as functions of the recoil energy, where CE ν NS process is drawn in solid lines while EvES is in dash lines.

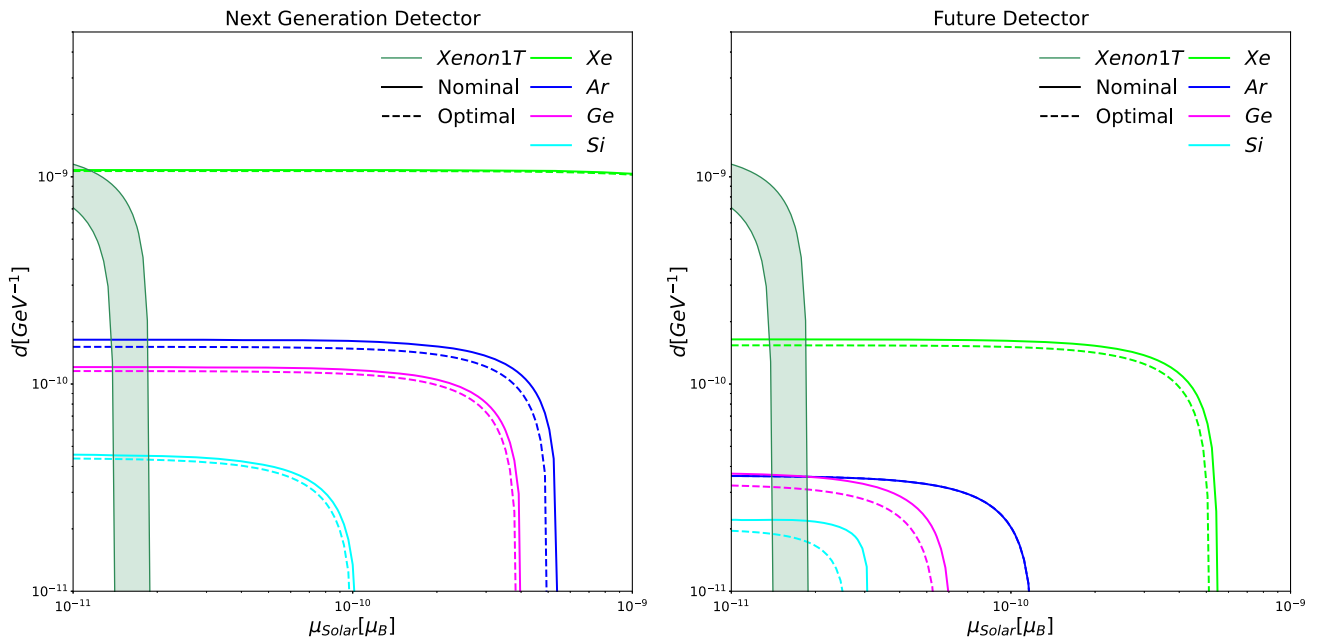


FIG. 6. 90% CL upper limits on the neutrino magnetic moments in the presence of both the ν_a MM, denoted as μ_s for solar neutrinos described in Eq. (2.10), and the ν_s MM in term of d with $m_4 = 1$ MeV from the experimental scenarios listed in Table I, where the solid lines are for the nominal systematic uncertainty and dashed lines for the optimal systematic uncertainty. The left and right panels are shown for the next generation and future experimental scenarios, respectively. A weighted average have been performed according to the natural abundance of isotopes in the detector materials. We also show the allowed parameter space to explain the Xenon1T excess [66].

further research in the future. An extremely large exposure may also help to keep the threshold in a practical range, which is considered in Ref. [126].

Finally, we study the general framework in the presence of both the ν_s MM and ν_a MM and illustrate the sensitivity in Fig. 6 by fixing $m_4 = 1$ MeV. We show the constraints on both ν_s MM and ν_a MM with different experimental scenarios, together with the allowed parameter space to explain the Xenon1T excess [66]. It is observed that both next generation and future DD experiments except xenon-based ones can exclude the allowed range of the ν_s MM with $d \gtrsim 10^{-10}$ GeV $^{-1}$. However, none of the experimental scenarios could exclude the region of $d < 10^{-11}$ GeV $^{-1}$ where the ν_a MM dominates the contribution to the Xenon1T excess. In this respect, other probes, such as the $E\nu$ ES process, are needed to test the explanation of the Xenon1T excess.

V. CONCLUSION

The dark matter DD experiments are entering the multi-ton scale phase, which also have great potential to detect the solar neutrino CE ν NS process. In this work, we have presented the detection potential of the ν_a MM and ν_s MM in the solar neutrino CE ν NS process in the next generation and future DD experiments. We have illustrated the sensitivity of the ν_a MM and ν_s MM, and compared with

the respective allowed range of the Xenon1T excess and other experimental constraints. We find that the ν_a MM sensitivity lies in the levels of $[10^{-10}, 10^{-11}] \mu_B$, which is dominantly limited by the detection threshold. Only future silicon based experiments could test the allowed region of the Xenon1T excess. On the other hand, the solar neutrino CE ν NS process is powerful to probe the ν_s MM for the sterile neutrino mass below 10 MeV. All the considered scenarios can unambiguously test the ν_s MM explanation of the Xenon1T excess with at least one order of magnitude better detection sensitivities. Finally, we have also derived the detection potential in the general framework with both ν_a MM and ν_s MM contributions in the CE ν NS. Therefore we conclude that the future the solar neutrino CE ν NS detection would be a new and promising tool to test new physics beyond the SM.

ACKNOWLEDGMENTS

Y.-F.L. is grateful to Dr. Jing-yu Zhu for helpful discussions on models of the neutrino dipole portal. The work of Y.-F.L. and S.-Y.X. was supported by National Natural Science Foundation of China under Grants No. 12075255, No. 12075254, and No. 11835013, by the Key Research Program of the Chinese Academy of Sciences under Grant No. XDPB15.

-
- [1] D. Z. Freedman, Coherent neutrino nucleus scattering as a probe of the weak neutral current, *Phys. Rev. D* **9**, 1389 (1974).
 - [2] D. Z. Freedman, D. N. Schramm, and D. L. Tubbs, The weak neutral current and its effects in stellar collapse, *Annu. Rev. Nucl. Part. Sci.* **27**, 167 (1977).
 - [3] D. Akimov *et al.* (COHERENT Collaboration), Observation of coherent elastic neutrino-nucleus scattering, *Science* **357**, 1123 (2017).
 - [4] D. Akimov *et al.* (COHERENT Collaboration), First Measurement of Coherent Elastic Neutrino-Nucleus Scattering on Argon, *Phys. Rev. Lett.* **126**, 012002 (2021).
 - [5] D. Akimov *et al.*, Measurement of the Coherent Elastic Neutrino-Nucleus Scattering Cross Section on CsI by COHERENT, *Phys. Rev. Lett.* **129**, 081801 (2022).
 - [6] P. Coloma, M. C. Gonzalez-Garcia, M. Maltoni, and T. Schwetz, COHERENT enlightenment of the neutrino dark side, *Phys. Rev. D* **96**, 115007 (2017).
 - [7] J. Liao and D. Marfatia, COHERENT constraints on nonstandard neutrino interactions, *Phys. Lett. B* **775**, 54 (2017).
 - [8] D. K. Papoulias and T. S. Kosmas, COHERENT constraints to conventional and exotic neutrino physics, *Phys. Rev. D* **97**, 033003 (2018).
 - [9] P. B. Denton, Y. Farzan, and I. M. Shoemaker, Testing large non-standard neutrino interactions with arbitrary mediator mass after COHERENT data, *J. High Energy Phys.* **07** (2018) 037.
 - [10] D. Aristizabal Sierra, V. De Romeri, and N. Rojas, COHERENT analysis of neutrino generalized interactions, *Phys. Rev. D* **98**, 075018 (2018).
 - [11] M. Cadeddu, C. Giunti, Y. F. Li, and Y. Y. Zhang, Average CsI Neutron Density Distribution from COHERENT Data, *Phys. Rev. Lett.* **120**, 072501 (2018).
 - [12] D. K. Papoulias, T. S. Kosmas, R. Sahu, V. K. B. Kota, and M. Hota, Constraining nuclear physics parameters with current and future COHERENT data, *Phys. Lett. B* **800**, 135133 (2020).
 - [13] C. Giunti and A. Studenikin, Neutrino electromagnetic interactions: A window to new physics, *Rev. Mod. Phys.* **87**, 531 (2015).
 - [14] C. Giunti, K. A. Kouzakov, Y. F. Li, A. V. Lokhov, A. I. Studenikin, and S. Zhou, Electromagnetic neutrinos in laboratory experiments and astrophysics, *Ann. Phys. (Berlin)* **528**, 198 (2016).
 - [15] M. Abdullah *et al.*, Coherent elastic neutrino-nucleus scattering: Terrestrial and astrophysical applications, in *2022 Snowmass Summer Study* (2022), arXiv:2203.07361.

- [16] V. Brdar, A. Greljo, J. Kopp, and T. Opferkuch, The neutrino magnetic moment portal: Cosmology, astrophysics, and direct detection, *J. Cosmol. Astropart. Phys.* **01** (2021) 039.
- [17] M. Cadeddu, F. Dordei, C. Giunti, Y. F. Li, E. Picciau, and Y. Y. Zhang, Physics results from the first COHERENT observation of coherent elastic neutrino-nucleus scattering in argon and their combination with cesium-iodide data, *Phys. Rev. D* **102**, 015030 (2020).
- [18] M. Cadeddu, N. Cargioli, F. Dordei, C. Giunti, Y. F. Li, E. Picciau, C. A. Ternes, and Y. Y. Zhang, New insights into nuclear physics and weak mixing angle using electroweak probes, *Phys. Rev. C* **104**, 065502 (2021).
- [19] E. Ciuffoli, J. Evslin, Q. Fu, and J. Tang, Extracting nuclear form factors with coherent neutrino scattering, *Phys. Rev. D* **97**, 113003 (2018).
- [20] P. Coloma, I. Esteban, M. C. Gonzalez-Garcia, and J. Menendez, Determining the nuclear neutron distribution from coherent elastic neutrino-nucleus scattering: Current results and future prospects, *J. High Energy Phys.* **08** (2020) 030.
- [21] M. Cadeddu and F. Dordei, Reinterpreting the weak mixing angle from atomic parity violation in view of the Cs neutron rms radius measurement from COHERENT, *Phys. Rev. D* **99**, 033010 (2019).
- [22] M. Cadeddu, C. Giunti, K. A. Kouzakov, Y. F. Li, A. I. Studenikin, and Y. Y. Zhang, Neutrino charge radii from COHERENT elastic neutrino-nucleus scattering, *Phys. Rev. D* **98**, 113010 (2018); **101**, 059902(E) (2020).
- [23] M. Cadeddu, F. Dordei, C. Giunti, Y. F. Li, and Y. Y. Zhang, Neutrino, electroweak, and nuclear physics from COHERENT elastic neutrino-nucleus scattering with refined quenching factor, *Phys. Rev. D* **101**, 033004 (2020).
- [24] J. E. Kim, A. Dasgupta, and S. K. Kang, Probing neutrino dipole portal at COHERENT experiment, *J. High Energy Phys.* **11** (2021) 120.
- [25] C. Giunti, General COHERENT constraints on neutrino nonstandard interactions, *Phys. Rev. D* **101**, 035039 (2020).
- [26] M. A. Corona, M. Cadeddu, N. Cargioli, F. Dordei, C. Giunti, Y. F. Li, E. Picciau, C. A. Ternes, and Y. Y. Zhang, Probing light mediators and $(g-2)_\mu$ through detection of coherent elastic neutrino nucleus scattering at COHERENT, *J. High Energy Phys.* **05** (2022) 109.
- [27] Y.-F. Li and S.-y. Xia, Constraining light mediators via detection of coherent elastic solar neutrino nucleus scattering, *Nucl. Phys.* **B977**, 115737 (2022).
- [28] P. S. Barbeau, Y. Efremenko, and K. Scholberg, COHERENT at the spallation neutron source, *arXiv:2111.07033*.
- [29] D. Baxter *et al.*, Coherent elastic neutrino-nucleus scattering at the european spallation source, *J. High Energy Phys.* **02** (2020) 123.
- [30] H. Bonet *et al.* (CONUS Collaboration), Constraints on Elastic Neutrino Nucleus Scattering in the Fully Coherent Regime from the CONUS Experiment, *Phys. Rev. Lett.* **126**, 041804 (2021).
- [31] H. Bonet *et al.* (CONUS Collaboration), Novel constraints on neutrino physics beyond the standard model from the CONUS experiment, *J. High Energy Phys.* **05** (2022) 085.
- [32] A. Aguilar-Arevalo *et al.* (CONNIE Collaboration), Search for light mediators in the low-energy data of the CONNIE reactor neutrino experiment, *J. High Energy Phys.* **04** (2020) 054.
- [33] A. Aguilar-Arevalo *et al.* (CONNIE Collaboration), Search for coherent elastic neutrino-nucleus scattering at a nuclear reactor with CONNIE 2019 data, *J. High Energy Phys.* **05** (2022) 017.
- [34] P. Coloma, I. Esteban, M. C. Gonzalez-Garcia, L. Larizgoitia, F. Monrabal, and S. Palomares-Ruiz, Bounds on new physics with data of the Dresden-II reactor experiment and COHERENT, *J. High Energy Phys.* **05** (2022) 037.
- [35] D. A. Sierra, V. De Romeri, and D. K. Papoulias, Consequences of the Dresden-II reactor data for the weak mixing angle and new physics, *J. High Energy Phys.* **09** (2022) 076.
- [36] R. F. Lang, C. McCabe, S. Reichard, M. Selvi, and I. Tamborra, Supernova neutrino physics with xenon dark matter detectors: A timely perspective, *Phys. Rev. D* **94**, 103009 (2016).
- [37] L. Pattavina, N. Ferreiro Iachellini, and I. Tamborra, Neutrino observatory based on archaeological lead, *Phys. Rev. D* **102**, 063001 (2020).
- [38] L. Pattavina *et al.* (RES-NOVA Collaboration), RES-NOVA sensitivity to core-collapse and failed core-collapse supernova neutrinos, *J. Cosmol. Astropart. Phys.* **10** (2021) 064.
- [39] N. Raj, Neutrinos from Type Ia and Failed Core-Collapse Supernovae at Dark Matter Detectors, *Phys. Rev. Lett.* **124**, 141802 (2020).
- [40] N. Raj, V. Takhistov, and S. J. Witte, Presupernova neutrinos in large dark matter direct detection experiments, *Phys. Rev. D* **101**, 043008 (2020).
- [41] X.-R. Huang, S. Zha, and L.-W. Chen, Supernova preshock neutronization burst as a probe of non-standard neutrino interactions, *Astrophys. J. Lett.* **923**, L26 (2021).
- [42] V. Munoz, V. Takhistov, S. J. Witte, and G. M. Fuller, Exploring the origin of supermassive black holes with coherent neutrino scattering, *J. Cosmol. Astropart. Phys.* **11** (2021) 020.
- [43] R. Calabrese, D. F. G. Fiorillo, G. Miele, S. Morisi, and A. Palazzo, Primordial black hole dark matter evaporating on the neutrino floor, *Phys. Lett. B* **829**, 137050 (2022).
- [44] P. Anselmann *et al.* (GALLEX Collaboration), Solar neutrinos observed by GALLEX at Gran Sasso, *Phys. Lett. B* **285**, 376 (1992).
- [45] M. Altmann *et al.* (GNO Collaboration), GNO solar neutrino observations: Results for GNO I, *Phys. Lett. B* **490**, 16 (2000).
- [46] A. I. Abazov *et al.*, Search for Neutrinos from Sun Using the Reaction Ga-71 (Electron-Neutrino e-) Ge-71, *Phys. Rev. Lett.* **67**, 3332 (1991).
- [47] J. N. Abdurashitov *et al.* (SAGE Collaboration), Measurement of the Solar Neutrino Capture Rate by Sage and Implications for Neutrino Oscillations in Vacuum, *Phys. Rev. Lett.* **83**, 4686 (1999).
- [48] B. T. Cleveland, T. Daily, R. Davis, Jr., J. R. Distel, K. Lande, C. K. Lee, P. S. Wildenhain, and J. Ullman (Homestake Collaboration), Measurement of the solar electron neutrino flux with the homestake chlorine detector, *Astrophys. J.* **496**, 505 (1998).

- [49] Q. R. Ahmad *et al.* (SNO Collaboration), Measurement of the Rate of $\nu_e + d \rightarrow p + p + e^-$ Interactions Produced by ^8B Solar Neutrinos at the Sudbury Neutrino Observatory, *Phys. Rev. Lett.* **87**, 071301 (2001).
- [50] Q. R. Ahmad *et al.* (SNO Collaboration), Direct Evidence for Neutrino Flavor Transformation from Neutral-Current Interactions in the Sudbury Neutrino Observatory, *Phys. Rev. Lett.* **89**, 011301 (2002).
- [51] S. N. Ahmed *et al.* (SNO Collaboration), Measurement of the Total Active ^8B Solar Neutrino Flux at the Sudbury Neutrino Observatory with Enhanced Neutral Current Sensitivity, *Phys. Rev. Lett.* **92**, 181301 (2004).
- [52] B. Aharmim *et al.* (SNO Collaboration), An Independent Measurement of the Total Active ^8B Solar Neutrino Flux Using an Array of ^3He Proportional Counters at the Sudbury Neutrino Observatory, *Phys. Rev. Lett.* **101**, 111301 (2008).
- [53] K. S. Hirata *et al.* (Kamiokande Collaboration), Observation of B-8 Solar Neutrinos in the Kamiokande-II Detector, *Phys. Rev. Lett.* **63**, 16 (1989).
- [54] S. Fukuda *et al.* (Super-Kamiokande Collaboration), Solar ^8B and *hep* Neutrino Measurements from 1258 Days of Super-Kamiokande Data, *Phys. Rev. Lett.* **86**, 5651 (2001).
- [55] C. Arpesella *et al.* (Borexino Collaboration), First real time detection of ^7B solar neutrinos by Borexino, *Phys. Lett. B* **658**, 101 (2008).
- [56] G. Bellini *et al.* (Borexino Collaboration), Measurement of the solar ^8B neutrino flux with 246 live days of Borexino and observation of the MSW vacuum-matter transition, *Phys. Rev. D* **82**, 033006 (2010).
- [57] G. Bellini *et al.* (Borexino Collaboration), First Evidence of *pep* Solar Neutrinos by Direct Detection in Borexino, *Phys. Rev. Lett.* **108**, 051302 (2012).
- [58] G. Bellini *et al.* (Borexino Collaboration), Neutrinos from the primary proton-proton fusion process in the sun, *Nature (London)* **512**, 383 (2014).
- [59] M. Agostini *et al.* (Borexino Collaboration), First direct experimental evidence of CNO neutrinos, *Nature (London)* **587**, 577 (2020).
- [60] C. Boehm, D. G. Cerdeño, P. A. N. Machado, A. Olivares-Del Campo, and E. Reid, How high is the neutrino floor?, *J. Cosmol. Astropart. Phys.* **01** (2019) 043.
- [61] M. C. Gonzalez-Garcia, M. Maltoni, Y. F. Perez-Gonzalez, and R. Zukanovich Funchal, Neutrino discovery limit of dark matter direct detection experiments in the presence of non-standard interactions, *J. High Energy Phys.* **07** (2018) 019.
- [62] D. K. Papoulias, R. Sahu, T. S. Kosmas, V. K. B. Kota, and B. Nayak, Novel neutrino-floor and dark matter searches with deformed shell model calculations, *Adv. High Energy Phys.* **2018**, 1 (2018).
- [63] W. Chao, J.-G. Jiang, X. Wang, and X.-Y. Zhang, Direct detections of dark matter in the presence of non-standard neutrino interactions, *J. Cosmol. Astropart. Phys.* **08** (2019) 010.
- [64] D. Aristizabal Sierra, V. De Romeri, L. J. Flores, and D. K. Papoulias, Impact of COHERENT measurements, cross section uncertainties and new interactions on the neutrino floor, *J. Cosmol. Astropart. Phys.* **01** (2022) 055.
- [65] C. A. J. O'Hare, Can we overcome the neutrino floor at high masses?, *Phys. Rev. D* **102**, 063024 (2020).
- [66] E. Aprile *et al.* (XENON Collaboration), Excess electronic recoil events in XENON1T, *Phys. Rev. D* **102**, 072004 (2020).
- [67] E. Aprile *et al.* (XENON Collaboration), Search for New Physics in Electronic Recoil Data from XENONnT, *Phys. Rev. Lett.* **129**, 161805 (2022).
- [68] O. G. Miranda, D. K. Papoulias, M. Tórtola, and J. W. F. Valle, XENON1T signal from transition neutrino magnetic moments, *Phys. Lett. B* **808**, 135685 (2020).
- [69] B. Yue, J. Liao, and J. Ling, Probing neutrino magnetic moment at the Jinping neutrino experiment, *J. High Energy Phys.* **08** (2021) 068.
- [70] M. Agostini *et al.* (The Borexino Collaboration), Limiting neutrino magnetic moments with Borexino Phase-II solar neutrino data, *Phys. Rev. D* **96**, 091103 (2017).
- [71] A. Córscico, L. Althaus, M. M. Bertolami, S. Kepler, and E. García-Berro, Constraining the neutrino magnetic dipole moment from white dwarf pulsations, *J. Cosmol. Astropart. Phys.* **08** (2014) 054.
- [72] F. Capozzi and G. Raffelt, Axion and neutrino bounds improved with new calibrations of the tip of the red-giant branch using geometric distance determinations, *Phys. Rev. D* **102**, 083007 (2020).
- [73] S. Arceo Díaz, K.-P. Schröder, K. Zuber, D. Jack, and E. E. Bricio Barrios, Constraint on the axion-electron coupling constant and the neutrino magnetic dipole moment by using the tip-RGB luminosity of fifty globular clusters, [arXiv:1910.10568](https://arxiv.org/abs/1910.10568).
- [74] G. Magill, R. Plestid, M. Pospelov, and Y.-D. Tsai, Dipole portal to heavy neutral leptons, *Phys. Rev. D* **98**, 115015 (2018).
- [75] P. Coloma, P. A. N. Machado, I. Martinez-Soler, and I. M. Shoemaker, Double-Cascade Events from New Physics in Icecube, *Phys. Rev. Lett.* **119**, 201804 (2017).
- [76] T. Schwetz, A. Zhou, and J.-Y. Zhu, Constraining active-sterile neutrino transition magnetic moments at DUNE near and far detectors, *J. High Energy Phys.* **07** (2021) 200.
- [77] M. Masip, P. Masjuan, and D. Meloni, Heavy neutrino decays at MiniBooNE, *J. High Energy Phys.* **01** (2013) 106.
- [78] E. Bertuzzo, S. Jana, P. A. N. Machado, and R. Zukanovich Funchal, Dark Neutrino Portal to Explain MiniBooNE excess, *Phys. Rev. Lett.* **121**, 241801 (2018).
- [79] I. M. Shoemaker and J. Wyenberg, Direct detection experiments at the neutrino dipole portal frontier, *Phys. Rev. D* **99**, 075010 (2019).
- [80] I. M. Shoemaker, Y.-D. Tsai, and J. Wyenberg, Active-to-sterile neutrino dipole portal and the XENON1T excess, *Phys. Rev. D* **104**, 115026 (2021).
- [81] R. Plestid, Luminous solar neutrinos I: Dipole portals, *Phys. Rev. D* **104**, 075027 (2021).
- [82] D. K. Papoulias, T. S. Kosmas, and Y. Kuno, Recent probes of standard and non-standard neutrino physics with nuclei, *Front. Phys.* **7**, 191 (2019).
- [83] A. B. Balantekin and N. Vassh, Magnetic moments of active and sterile neutrinos, *Phys. Rev. D* **89**, 073013 (2014).

- [84] H. Zhang *et al.* (PandaX Collaboration), Dark matter direct search sensitivity of the PandaX-4T experiment, *Sci. China Phys. Mech. Astron.* **62**, 31011 (2019).
- [85] J. Aalbers *et al.* (DARWIN Collaboration), DARWIN: Towards the ultimate dark matter detector, *J. Cosmol. Astropart. Phys.* **11** (2016) 017.
- [86] C. E. Aalseth *et al.* (DarkSide-20k Collaboration), DarkSide-20k: A 20 tonne two-phase LAr TPC for direct dark matter detection at LNGS, *Eur. Phys. J. Plus* **133**, 131 (2018).
- [87] R. Agnese *et al.* (SuperCDMS Collaboration), Projected sensitivity of the SuperCDMS SNOLAB experiment, *Phys. Rev. D* **95**, 082002 (2017).
- [88] Q. Arnaud *et al.* (EDELWEISS Collaboration), Optimizing EDELWEISS detectors for low-mass WIMP searches, *Phys. Rev. D* **97**, 022003 (2018).
- [89] A. Drukier and L. Stodolsky, Principles and applications of a neutral current detector for neutrino physics and astronomy, *Phys. Rev. D* **30**, 2295 (1984).
- [90] K. Patton, J. Engel, G. C. McLaughlin, and N. Schunck, Neutrino-nucleus coherent scattering as a probe of neutron density distributions, *Phys. Rev. C* **86**, 024612 (2012).
- [91] P. A. Zyla *et al.* (Particle Data Group), Review of particle physics, *Prog. Theor. Exp. Phys.* **2020**, 083C01 (2020).
- [92] R. H. Helm, Inelastic and elastic scattering of 187-Mev electrons from selected even-even nuclei, *Phys. Rev.* **104**, 1466 (1956).
- [93] I. Angeli and K. P. Marinova, Table of experimental nuclear ground state charge radii: An update, *At. Data Nucl. Data Tables* **99**, 69 (2013).
- [94] P. Vogel and J. Engel, Neutrino electromagnetic form factors, *Phys. Rev. D* **39**, 3378 (1989).
- [95] D. Aristizabal Sierra, O. G. Miranda, D. K. Papoulias, and G. S. Garcia, Neutrino magnetic and electric dipole moments: From measurements to parameter space, *Phys. Rev. D* **105**, 035027 (2022).
- [96] J. N. Bahcall and A. M. Serenelli, How do uncertainties in the surface chemical abundances of the Sun affect the predicted solar neutrino fluxes?, *Astrophys. J.* **626**, 530 (2005).
- [97] J. N. Bahcall, A. M. Serenelli, and S. Basu, New solar opacities, abundances, helioseismology, and neutrino fluxes, *Astrophys. J.* **621**, L85 (2005).
- [98] R. Essig, M. Sholapurkar, and T.-T. Yu, Solar neutrinos as a signal and background in direct-detection experiments searching for sub-GeV dark matter with electron recoils, *Phys. Rev. D* **97**, 095029 (2018).
- [99] G. Cowan, K. Cranmer, E. Gross, and O. Vitells, Asymptotic formulae for likelihood-based tests of new physics, *Eur. Phys. J. C* **71**, 1554 (2011); **73**, 2501(E) (2013).
- [100] E. Aprile *et al.* (XENON100 Collaboration), First Dark Matter Results from the XENON100 Experiment, *Phys. Rev. Lett.* **105**, 131302 (2010).
- [101] D. Akerib *et al.* (LUX Collaboration), First Results from the LUX Dark Matter Experiment at the Sanford Underground Research Facility, *Phys. Rev. Lett.* **112**, 091303 (2014).
- [102] A. Tan *et al.* (PandaX-II Collaboration), Dark Matter Results from First 98.7 Days of Data from the PandaX-II Experiment, *Phys. Rev. Lett.* **117**, 121303 (2016).
- [103] P. Agnes *et al.* (DarkSide Collaboration), DarkSide-50 532-day dark matter search with low-radioactivity argon, *Phys. Rev. D* **98**, 102006 (2018).
- [104] DEAP Collaboration, Search for dark matter with a 231-day exposure of liquid argon using DEAP-3600 at SNOLAB, *Phys. Rev. D* **100**, 022004 (2019).
- [105] E. Aprile *et al.* (XENON Collaboration), Projected WIMP sensitivity of the XENONnT dark matter experiment, *J. Cosmol. Astropart. Phys.* **11** (2020) 031.
- [106] D. S. Akerib *et al.* (LZ Collaboration), The LUX-ZEPLIN (LZ) experiment, *Nucl. Instrum. Methods Phys. Res., Sect. A* **953**, 163047 (2020).
- [107] J. Billard *et al.*, Direct detection of dark matter—APPEC committee report, *Rep. Prog. Phys.* **85**, 056201 (2022).
- [108] R. Agnese *et al.* (CDMS Collaboration), Dark Matter Search Results Using the Silicon Detectors of CDMS II, *Phys. Rev. Lett.* **111**, 251301 (2013).
- [109] R. Agnese *et al.* (SuperCDMS Collaboration), Search for Low-Mass WIMPs with SuperCDMS, *Phys. Rev. Lett.* **112**, 241302 (2014).
- [110] T. Aramaki (SuperCDMS Collaboration), Recent results from the second CDMSlite run and overview of the SuperCDMS SNOLAB project, *Proc. Sci. DSU2015* (2016) 030.
- [111] H. Jiang *et al.*, Limits on Light WIMPs from the First 102.8 Kg-Days Data of the CDEX-10 Experiment, *Phys. Rev. Lett.* **120**, 241301 (2018).
- [112] M. Traina *et al.* (DAMIC Collaboration), Results on low-mass weakly interacting massive particles from a 11 kg d target exposure of DAMIC at SNOLAB, *Proc. Sci. ICRC2021* (2021) 539 [arXiv:2108.05983].
- [113] L. Barak *et al.* (SENSEI Collaboration), SENSEI: Direct-Detection Results on Sub-GeV Dark Matter from a New Skipper-CCD, *Phys. Rev. Lett.* **125**, 171802 (2020).
- [114] J. Tiffenberg, M. Sofo-Haro, A. Drlica-Wagner, R. Essig, Y. Guardincerri, S. Holland, T. Volansky, and T.-T. Yu (SENSEI Collaboration), Single-Electron and Single-Photon Sensitivity with a Silicon Skipper CCD, *Phys. Rev. Lett.* **119**, 131802 (2017).
- [115] C. Macolino (DARWIN Collaboration), DARWIN: Direct dark matter search with the ultimate detector, *J. Phys.* **1468**, 012068 (2020).
- [116] J. Lindhard, V. Nielsen, M. Scharff, and P. V. Thomsen, Integral equations governing radiation effects. (notes on atomic collisions, iii), *Kgl. Danske Videnskab., Selskab. Mat. Fys. Medd.* **33**, 31 (1963).
- [117] L. Wang and D. M. Mei, A comprehensive study of low-energy response for xenon-based dark matter experiments, *J. Phys. G* **44**, 055001 (2017).
- [118] O. G. Miranda, D. K. Papoulias, O. Sanders, M. Tórtola, and J. W. F. Valle, Low-energy probes of sterile neutrino transition magnetic moments, *J. High Energy Phys.* **12** (2021) 191.
- [119] M. Deniz *et al.* (TEXONO Collaboration), Measurement of Nu(e)-bar-electron scattering cross-section with a CsI (TI) scintillating crystal array at the Kuo-Sheng nuclear power reactor, *Phys. Rev. D* **81**, 072001 (2010).
- [120] D. W. Amaral *et al.* (SuperCDMS Collaboration), Constraints on low-mass, relic dark matter candidates from a

- surface-operated SuperCDMS single-charge sensitive detector, *Phys. Rev. D* **102**, 091101 (2020).
- [121] E. Aprile *et al.* (XENON Collaboration), Search for Coherent Elastic Scattering of Solar ^8B Neutrinos in the XENON1T Dark Matter Experiment, *Phys. Rev. Lett.* **126**, 091301 (2021).
- [122] S.-F. Ge, P. Pasquini, and J. Sheng, Solar active-sterile neutrino conversion with atomic effects at dark matter direct detection experiments, *J. High Energy Phys.* **05** (2022) 088.
- [123] B. M. Roberts, V. A. Dzuba, V. V. Flambaum, M. Pospelov, and Y. V. Stadnik, Dark matter scattering on electrons: Accurate calculations of atomic excitations and implications for the DAMA signal, *Phys. Rev. D* **93**, 115037 (2016).
- [124] R. Catena, T. Emken, N. A. Spaldin, and W. Tarantino, Atomic responses to general dark matter-electron interactions, *Phys. Rev. Res.* **2**, 033195 (2020).
- [125] K. A. Kouzakov, A. I. Studenikin, and M. B. Voloshin, Neutrino-impact ionization of atoms in searches for neutrino magnetic moment, *Phys. Rev. D* **83**, 113001 (2011).
- [126] Z. Ye, F. Zhang, D. Xu, and J. Liu, Unambiguously resolving the potential neutrino magnetic moment signal at large liquid scintillator detectors, *Chin. Phys. Lett.* **38**, 111401 (2021).